Electrochemistry Communications 100 (2019) 121–125

Contents lists available at ScienceDirect

Electrochemistry Communications

journal homepage: www.elsevier.com/locate/elecom

High entropy oxides as anode material for Li-ion battery applications: A practical approach

Qingsong Wang[a,*], Abhishek Sarkar[a,b], Zhenyou Li[a,c], Yang Lu[d], Leonardo Velasco[a], Subramshu S. Bhattacharya[e], Torsten Brezesinski[a], Horst Hahn[a,c], Ben Breitung[a,f,**]

[a] Institute of Nanotechnology, Karlsruhe Institute of Technology (KIT), Hermann-von-Helmholtz-Platz 1, 76344 Eggenstein-Leopoldshafen, Germany
[b] Technische Universität Darmstadt, KIT-TUD Joint Laboratory Nanomaterials, 64247 Darmstadt, Germany
[c] Helmholtz Institute Ulm for Electrochemical Energy Storage, Helmholtzstrasse 11, 89081 Ulm, Germany
[d] CAS Key Laboratory of Materials for Energy Conversion, Shanghai Institute of Ceramics, Chinese Academy of Sciences, Shanghai, PR China
[e] Nano-Functional Material Technology Centre (NFMTC), Department of Metallurgical and Materials Engineering, Indian Institute of Technology Madras, Chennai, 600036, India
[f] Karlsruhe Nano Micro Facility, Karlsruhe Institute of Technology (KIT), Hermann-von-Helmholtz-Platz 1, 76344 Eggenstein-Leopoldshafen, Germany

ARTICLE INFO

Keywords:
Lithium-ion battery
Full-cell
High entropy oxide anode
NCM111 cathode
Three-electrode cyclic voltammetry

ABSTRACT

Owing to their robust Li-ion storage properties induced by the entropy stabilization effect, transition-metal-based high entropy oxides are considered promising electrode materials for use in Li-ion batteries. In this work, full-cells comprising $(Co_{0.2}Cu_{0.2}Mg_{0.2}Ni_{0.2}Zn_{0.2})O$ anode and $LiNi_{1/3}Co_{1/3}Mn_{1/3}O_2$ cathode were assembled to explore their potential for practical applications. The cycling performance was studied by different electrochemical experiments. The cells were found to deliver an initial specific discharge capacity of 446 mAh g^{-1}, which was maintained at 300 and 256 mAh g^{-1} after 50 and 100 cycles, respectively, and they showed stable cyclability even at specific currents of 1.6 A g^{-1}. More importantly, high specific energy and power densities of about 240 Wh kg^{-1} and 320 W kg^{-1} were achieved. Additionally, pouch cells of total capacity 2.5 mAh were built and successfully employed as a power source.

1. Introduction

In recent years, transition-metal oxides (TMOs) have been widely tested as electrode materials for next-generation lithium-ion batteries (LIBs) [1–4]. The conversion reaction mechanism in TMOs for anode applications enables multi-electron redox processes rather than only one-electron exchange, thereby offering large theoretical specific capacities (> 1000 mAh g^{-1}) [5–9]. Moreover, in comparison to graphite anodes, TMOs have been shown to operate at relatively higher voltages, which might be beneficial in terms of safety, as there is a lower risk of short circuiting due to Li-plating [10]. However, conventional TMOs suffer from rapid capacity fading due to severe structural changes associated with the large volume expansion/contraction with cycling, among others [11–13].

Very recently, it has been discovered that transition-metal-based high entropy oxides (TM-HEOs) exhibit robust (and reversible) lithium storage properties, and it was demonstrated that the improvements in cycling stability are due to entropy stabilization [14,15]. The concept of entropy stabilization of multicomponent compounds was first applied to high entropy alloys, where more than five different metals form a single-phase crystal structure [16]. The same concept was then applied to different types of oxides, with the most widely studied TM-HEO being $(Co_{0.2}Cu_{0.2}Mg_{0.2}Ni_{0.2}Zn_{0.2})O$ [17–22]. Different from conventional TMOs, the entropy-stabilized crystal structure is believed to serve as a kind of host matrix for the conversion reaction and was found to be partially retained even in the fully lithiated state [14,15].

At present, layered lithium transition-metal oxides of NCM type ($Li[Ni_xCo_yMn_{1-x-y}]O_2$) are one of the most promising cathode material families for application in high-energy-density LIBs [23]. Solid solutions of $LiCoO_2$, $LiNiO_2$ and $LiMnO_2$ typically show improved kinetics (cobalt) and specific capacity (nickel) as well as better safety characteristics (manganese) compared to the ternary oxide endmembers [24]. $LiNi_{1/3}Co_{1/3}Mn_{1/3}O_2$ (NCM111) cells have been frequently reported to show long-term cycling stability, with specific capacities

* Corresponding author.
** Correspondence to: B. Breitung, Institute of Nanotechnology, Karlsruhe Institute of Technology (KIT), Hermann-von-Helmholtz-Platz 1, 76344 Eggenstein-Leopoldshafen, Germany.
E-mail addresses: qingsong.wang@kit.edu (Q. Wang), ben.breitung@kit.edu (B. Breitung).

https://doi.org/10.1016/j.elecom.2019.02.001
Received 10 January 2019; Received in revised form 1 February 2019; Accepted 2 February 2019
Available online 04 February 2019

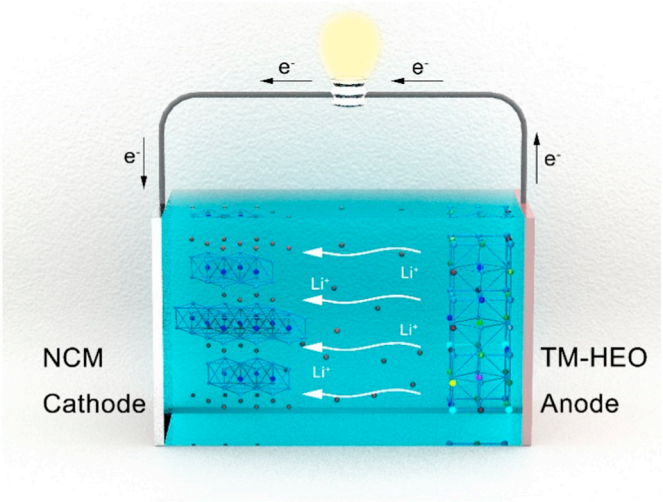

Fig. 1. Schematic figure of the full-cell using NCM111 cathode and TM-HEO anode. During charge, Li ions migrate from the cathode to the anode, with electron flow in the same direction through the outer circuit, and deintercalation and conversion reactions occurring at the positive and negative electrode, respectively. On discharge, the reverse happens.

around 150 mAh g^{-1}, and offer the possibility for an extended operating voltage range when cycled against Li metal [25,26]. Hence, state-of-the-art NCM111 was chosen as the cathode active material here to explore the applicability of TM-HEO in full-cells. Of note, in half-cells with a Li counter electrode, there is always excess Li available. However, in full-cell configurations, the cathode material is usually the only source of Li ions. Consequently, consumption processes (predominantly at the anode side due to e.g., solid electrolyte interphase [SEI] formation) in the first few cycles will substantially decrease the Li fraction [27]. For that reason, accurate balancing between the cathode and the anode is clearly necessary to ensure high TM-HEO utilization over many cycles.

In this work, systematic electrochemical characterization of TM-HEO in full-cells with an NCM111 cathode was carried out. Anode and cathode potentials (vs. Li^+/Li) were individually monitored using three-electrode Swagelok cells. Furthermore, we discuss the cycling behavior and rate capability of full-cells as well as the performance of NCM111//TM-HEO pouch cells. A schematic figure of the cell configuration is depicted in Fig. 1, together with the crystal structures of both electrode materials used.

2. Experimental

TM-HEO powder was prepared by nebulized spray pyrolysis, which is a facile and scalable synthesis technique with a (laboratory) production rate of 1–2 g h^{-1} for homogeneous nanocrystalline materials. An ultrasonic nebulizer was used to produce metal-nitrate precursor mist containing fine droplets, which were carried by flowing oxygen through a tube furnace, where TM-HEO powder was formed at 1150 °C. More details about the synthesis can be found elsewhere. [14,20] Electrode slurries for the preparation of anode sheets were made by high-energy dispersion (Thinky mixer ARE-250, 3 min, 2000 rpm) of appropriate amounts of 7:2:1 by weight TM-HEO, Super P carbon black additive and polyvinylidene fluoride (PVDF) binder (7.5 wt%) in *N*-methyl-2-pyrrolidone (NMP). The resulting slurries were pasted on a Cu foil via doctor-blading and then dried in a vacuum oven at 80 °C for 12 h. Preparation of cathode sheets was executed in a similar manner. Appropriate amounts of 8:1:1 by weight NCM111 (BASF SE, Ludwigshafen, Germany), Super P carbon black additive and PVDF binder were dispersed in NMP. The resulting slurries were cast onto an Al foil. After coating, the electrode sheets were dried at 80 °C. Electrode discs of diameter 13 mm were cut from the anode and cathode tapes. The electrodes were further dried under vacuum at 100 °C for at least 2 h and then transferred to an Ar-filled glove box (MBraun) with H_2O and O_2 contents of < 0.5 ppm, without any exposure to air. The areal loadings were around 2.8 mg_{NCM111} cm^{-2} and 0.7 $mg_{TM\text{-}HEO}$ cm^{-2}. CR2032-type coin cells were assembled inside the glove box. The electrolyte used was 1 M $LiPF_6$ in 3:7 by weight ethylene carbonate/ethyl methyl carbonate (Selectilyte LP57, BASF SE). Whatman™ GF/C glass microfiber filter paper of diameter 17 mm was used as the separator. For half-cells, Li metal was used as the counter electrode. Pouch cells with 2.2 × 4.2 cm^2 TM-HEO negative electrode and 2.0 × 4.0 cm^2 NCM111 positive electrode were assembled for purpose of practical applications. In this case, Celgard 2500 was used as the separator. Galvanostatic measurements were performed on an Arbin battery test system (BT-2000) at both 25 °C and 45 °C. Swagelok T-cells (three-electrode configuration with a Li reference electrode) were also built and tested. Cyclic voltammetric experiments were performed on a Bio-logic potentiostat (VMP3). The specific capacities of full-cells were calculated based on the weight of TM-HEO.

3. Results and discussion

The as-prepared TM-HEO (mostly hollow spherical particle morphology) displays a single-phase rock-salt structure (*Fm*-3*m*), and the corresponding scanning transmission electron microscopy (STEM) elemental maps demonstrate the homogenous elemental distribution (Fig. S1). NCM111 (spherical secondary particles assembled from primary particles of size 200–500 nm) exhibits the typical layered crystal structure with *R*-3*m* space group (Fig. S1). Details about the cyclability of TM-HEO in half-cells are reported elsewhere [14,15]. Although the conversion mechanism of TM-HEO is still under debate, we believe that the general process—supported by TEM and operando X-ray diffraction (XRD)—can be described as follows: The entropy-stabilized rock-salt structure is partially preserved over the entire lithiation cycles, resulting in lower than theoretical specific capacities, since not every single cation is actively involved in the redox reactions, but significantly improved long-term cycling performance. During oxidation of TMs, the lattice structure serves as a kind of host matrix and facilitates their reintegration.

The as-assembled NCM111//TM-HEO full-cells revealed an open-circuit voltage of 0.3–0.5 V, corresponding to the discharged state and being a direct result of potential differences between the TM-HEO and the NCM111 (TM-HEO//Li: 2.78 V, NCM111//Li: 3.22 V; see Fig. 2a). Taking into account the stable specific capacities of about 600 mAh g^{-1} and 150 mAh g^{-1} for TM-HEO and NCM111, respectively, the properly balanced cathode/anode active material weight ratio is about four. Accordingly, the areal loadings were adjusted to 2.8 mg_{NCM111} cm^{-2} and 0.7 $mg_{TM\text{-}HEO}$ cm^{-2}. Fig. 2b shows cyclic voltammograms (CV) for the first three cycles of an NCM111//TM-HEO full-cell. CV data were collected in the voltage range between 0.5 and 4.5 V at a sweep rate of 0.1 mV s^{-1}. In the first cycle, a large peak appeared at about 3.1 V (0.71 V vs. Li^+/Li for TM-HEO), which can be clearly attributed to the reduction of TM-HEO. This finding is in good agreement with the initial lithiation of TM-HEO, which was found to occur at potentials below 0.8 V in half-cells (Fig. 2a). As expected, this peak at 3.1 V didn't reappear in the subsequent cycles, characteristic of conversion-type TMOs, where irreversible reactions such as pulverization and SEI formation, to name a few, predominantly take place in the first cycle [1,10,12,28].

The evolution of cathode and anode potentials was followed individually and simultaneously using a three-electrode setup, as shown in Fig. 2c. An increase in cut-off potentials during the course of cycling was noticed. This shift, which will be discussed in some more detail below, narrows the effective operating voltage range, thereby resulting in capacity decay.

Galvanostatic testing of NCM111//TM-HEO full-cells was performed at 25 °C in the same voltage range of 0.5–4.5 V. Charging and

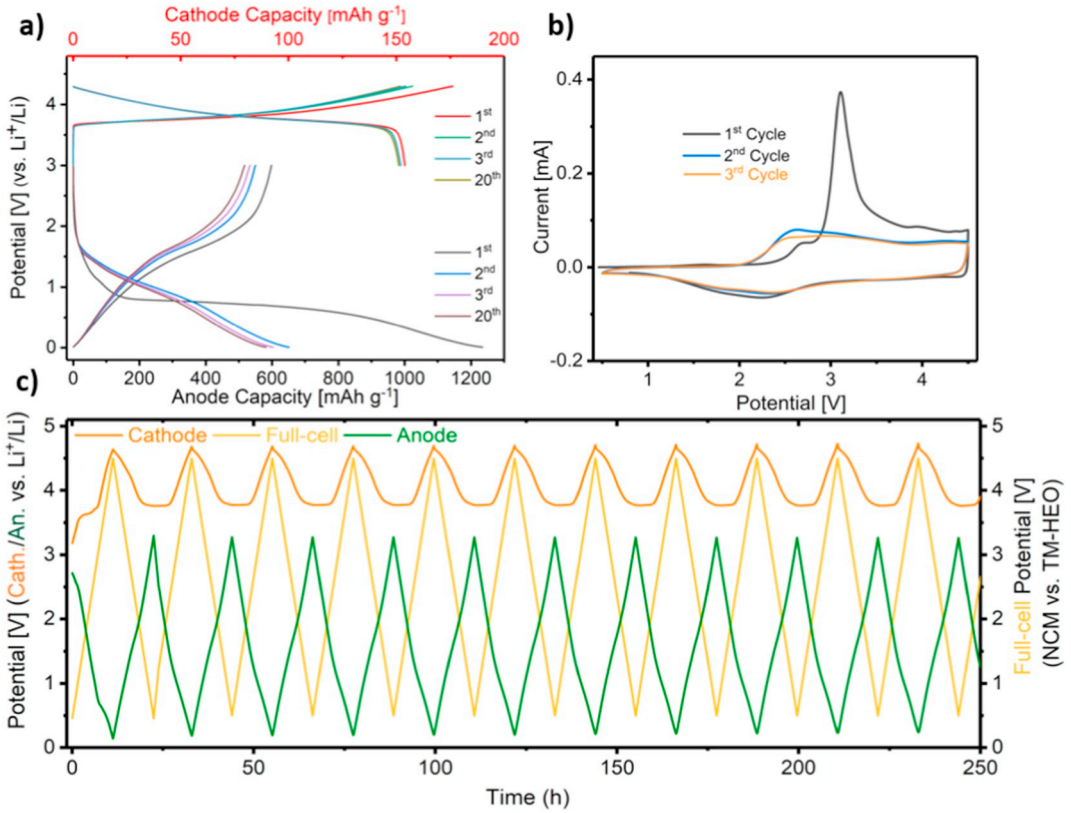

Fig. 2. a) Initial galvanostatic charge/discharge profiles of NCM111 cathode and TM-HEO anode in half-cells. b) CV curves (three-electrode configuration) in the voltage range between 0.5 and 4.5 V obtained on the NCM111//TM-HEO full-cell. The sweep rate was 0.1 mV s^{-1}. c) Full-cell potential and the corresponding cathode and anode potentials vs. Li^+/Li.

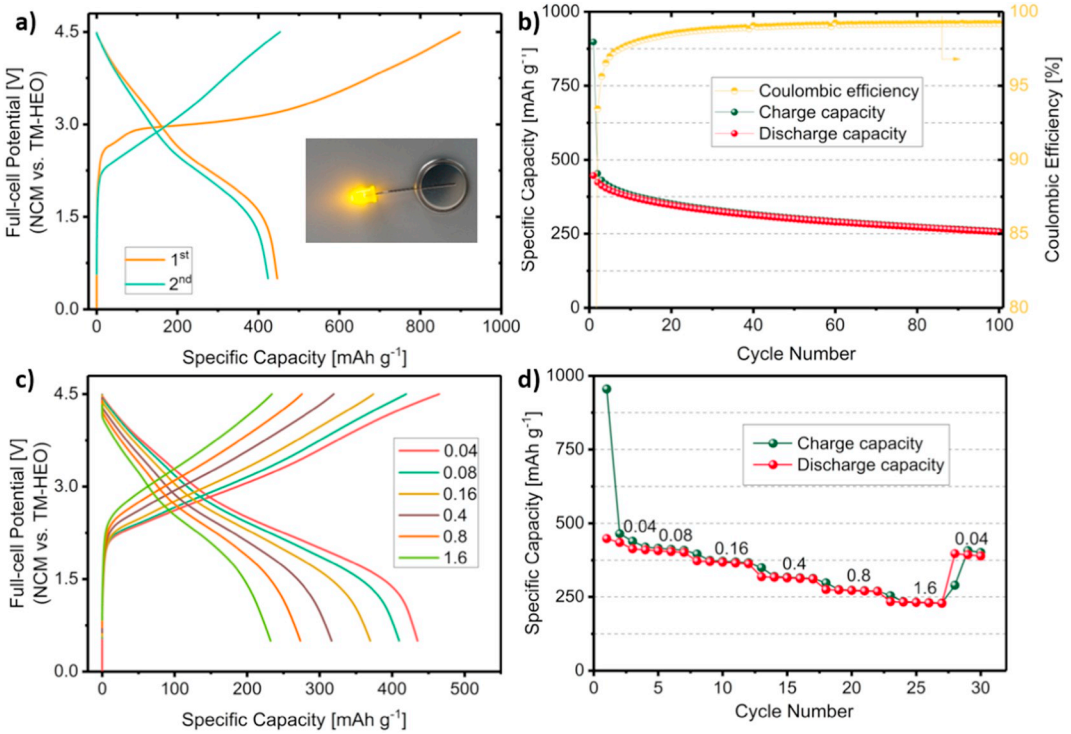

Fig. 3. Cycling performance of NCM111//TM-HEO full-cells at 25 °C and in the voltage range of 0.5–4.5 V. a) First and second cycle charge/discharge profiles. The inset is a photograph of an LED powered by a coin-type full-cell. b) Capacity retention at a specific current of 0.12 A g^{-1}. c) Charge/discharge profiles at different specific currents and d) rate capability. The current in c) and d) is given in units of A g^{-1}.

discharging corresponds to lithiation and delithiation of the TM-HEO anode, respectively. As is evident from Fig. 3a, a large specific capacity of about 900 mAh g^{-1} was achieved in the first charge cycle at a specific current of 0.12 A g^{-1}. Note that the capacity was calculated based on the weight of TM-HEO. Since the cathode capacity is the limiting factor in this case, the initial specific capacity is lower than that of TM-HEO in half-cells. A first cycle specific discharge capacity of 446 mAh g^{-1} was achieved, with an average discharge voltage of 2.65 V. Hence, a specific energy density of 236 Wh kg^{-1} (based on the total weight of cathode and anode active materials) can be reached. This value is higher than the energy density of full-cells using FeO_x-based conversion anodes (≈150 Wh kg^{-1}) and exceeds that of most cell systems listed in Table S1 [29–35]. The inset of Fig. 3a shows an LED powered by a coin-type full-cell when initially charged to 3.0 V. The cycling performance is displayed in Fig. 3b. Specific discharge capacities of 300 and 256 mAh g^{-1} were maintained after 50 and 100 cycles, respectively, with a capacity fade rate of 0.65% per cycle. The capacity degradation can be attributed in part to a shift of the effective operating voltage window, as can be seen in Fig. 2c [36]. The maximum (cut-off) potential of the NCM cathode (vs. Li^+/Li) increased from 4.64 to 4.73 V after 10 cycles. Since the working voltage of the full-cell was set at 4.0 V, the lower cut-off potential increased as well, thus resulting in capacity loss (see Fig. S2 for more details) [37]. Of note, high cut-off potentials on charge have been reported to be detrimental to the structural stability/integrity of NCM cathode materials [38,39].

The Coulombic efficiency in the initial cycle was around 50% because of irreversible loss of lithium. Nevertheless, in the subsequent cycles, the Coulombic efficiency stabilized well above 99%, enabled by the entropy stabilization effect. Figs. 3c and d depict the rate capability of NCM111//TM-HEO full-cells by applying specific currents ranging from 0.04 A g^{-1} to 1.6 A g^{-1}. The increasing voltage drop (overpotential) with increasing current is due to Ohmic polarization, which is often seen in cells using conversion anodes and intercalation cathodes [31]. Noteworthy, the specific capacity delivered at 1.6 A g^{-1} (234 mAh g^{-1}) was still 85% of that at 0.8 A g^{-1} (275 mAh g^{-1}), indicating good rate performance. Besides, the full-cell retained its original capacity when the applied current was set back to 0.04 A g^{-1}.

Testing at elevated temperature (45 °C) was also carried out to gain further insight into the kinetics of the electrochemical reaction. Interestingly, the cells showed similar cycling performance at 25 and 45 °C (Fig. S3). On the positive side, accelerated capacity degradation with increasing temperature was not apparent, which is beneficial for real-world applications [40].

Finally, upscaling was done in order to demonstrate the practical application potential of the NCM111//TM-HEO system. To this end, pouch cells (2 × 4 cm^2 electrode area) of similar areal loading to the coin-type cells described before were built and tested electrochemically. The first five cycles of cell charging and discharging are depicted in Fig. 4a. A stable discharge capacity of 2.5 mAh was achieved and utilized to supply electrical energy to an array of LEDs. After charging to 4.0 V, the pouch cell was connected to the LED array shown in the inset of Fig. 4a (32 LEDs working at a potential of 2 V and current of 64 mA). Electrochemical impedance spectroscopy (Fig. S4) demonstrated a small impedance (< 10 Ω) of the pouch cell. Constant load discharging (CLD) tests were conducted by connecting the LED array and the load serially while following the current flow through the array. For each cycle, the pouch cell was recharged to 4.0 V before doing the CLD testing. As in evident from Fig. 4b, by applying different resistances of 20, 40 and 60 Ω, initial currents of 146, 73 and 50 mA, respectively, were measured, thus emphasizing the reversibility of the (pouch) full-cell.

As previously mentioned, the initial lithium loss, mainly due to anode conversion, could not be recovered in the following cycles. In order to optimize the Li utilization in full-cells, a formation process was applied to the TM-HEO anode. To this end, TM-HEO//Li half-cells were discharged (lithiation process) to 0.01 V and charged (delithiation process) to 3.0 V vs. Li^+/Li for five consecutive cycles. After cell formation, the TM-HEO anodes were harvested and then assembled—together with NCM111 cathodes—to full-cells. Now, a discharge capacity of 450 mAh g^{-1} was achieved, even for a much smaller voltage range of 0.5–4.0 V (Fig. S5a). Three-electrode CV tests revealed only marginal shifts in potential (Fig. S5b). It should be noted that lower charge cut-off voltages offer the advantage of better keeping the NCM111 lattice structure intact [38,39]. Therefore, pre-lithiation (or pre-cycling), a common approach to optimize Li utilization when using conversion-type electrode materials in full-cells, is also applicable to high entropy oxides [41].

4. Conclusion

In summary, $(Co_{0.2}Cu_{0.2}Mg_{0.2}Ni_{0.2}Zn_{0.2})O$ has been successfully exploited as a negative electrode material in full-cells with a $LiNi_{1/3}Co_{1/3}Mn_{1/3}O_2$ cathode. A specific discharge capacity of 446 mAh g^{-1} was achieved in the first cycle and maintained at 300 mAh g^{-1} even after 50 cycles. Pouch cells with a total capacity of 2.5 mAh were built and successfully used as a power source to supply electricity to 32 LEDs. Further studies on the optimization of energy density by taking advantage of the large anode capacity are currently in progress. Because of the good cycling stability observed, even for non-optimized NCM111//TM-HEO cells, we believe that high entropy oxides, in general, hold potential as alternative electrode materials for next-generation Li-ion batteries.

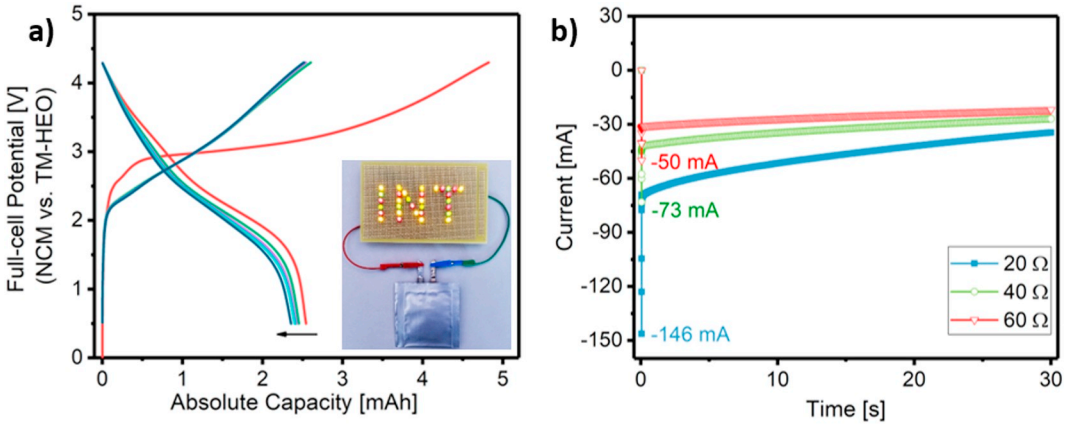

Fig. 4. a) Charge/discharge profiles of a pouch cell in the voltage range of 0.5–4.3 V. The specific current was 0.03 A g^{-1}. Increasing cycle number is denoted by the arrow. The inset is a photograph of an LED array powered by the pouch cell. b) Constant load discharging tests performed by connecting the LED array and the load serially.

Conflicts of interest

There are no conflicts to declare.

Acknowledgments

The authors acknowledge financial support from the Helmholtz Association and by the Deutsche Forschungsgemeinschaft (DFG) under project HA/1344/43-1. Financial support by EnABLES is also acknowledged. EnABLES has received funding from the European Union's Horizon 2020 research and innovation programme under grant agreement no. 730957. We acknowledge support by Deutsche Forschungsgemeinschaft and Open Access Publishing Fund of Karlsruhe Institute of Technology.

Appendix A. Supplementary data

Supplementary data to this article can be found online at https://doi.org/10.1016/j.elecom.2019.02.001.

References

[1] Y. Lu, L. Yu, X.W. Lou, Nanostructured conversion-type anode materials for advanced Lithium-ion batteries, Chem. 4 (2018) 972–996, https://doi.org/10.1016/j.chempr.2018.01.003.
[2] S. Zheng, X. Li, B. Yan, Q. Hu, Y. Xu, X. Xiao, H. Xue, H. Pang, Transition-metal (Fe, Co, Ni) based metal-organic frameworks for electrochemical energy storage, Adv. Energy Mater. 7 (2017) 1–27, https://doi.org/10.1002/aenm.201602733.
[3] X. Guo, S. Zheng, G. Zhang, X. Xiao, X. Li, Y. Xu, H. Xue, H. Pang, Nanostructured graphene-based materials for flexible energy storage, Energy Storage Mater. 9 (2017) 150–169, https://doi.org/10.1016/j.ensm.2017.07.006.
[4] X. Li, J. Wei, Q. Li, S. Zheng, Y. Xu, P. Du, C. Chen, J. Zhao, H. Xue, Q. Xu, H. Pang, Nitrogen-doped cobalt oxide nanostructures derived from cobalt–alanine complexes for high-performance oxygen evolution reactions, Adv. Funct. Mater. 28 (2018) 1–7, https://doi.org/10.1002/adfm.201800886.
[5] Y. Qian, P. Niehoff, D. Zhou, R. Adam, D. Mikhailova, M. Pyschik, M. Börner, R. Klöpsch, D. Rafaja, G. Schumacher, H. Ehrenberg, M. Winter, F. Schappacher, Investigation of nano-sized Cu(II)O as a high capacity conversion material for Li-metal cells and lithium-ion full cells, J. Mater. Chem. A 5 (2017) 6556–6568, https://doi.org/10.1039/C6TA10944F.
[6] G.E. Blomgren, The development and future of lithium ion batteries, J. Electrochem. Soc. 164 (2017) A5019–A5025, https://doi.org/10.1149/2.0251701jes.
[7] Y. Lu, J. Nai, X.W. Lou, Formation of $NiCo_2V_2O_8$Yolk–double shell spheres with enhanced lithium storage properties, Angew. Chem. Int. Ed. 57 (2018) 2899–2903, https://doi.org/10.1002/anie.201800363.
[8] S.L. Zhang, B.Y. Guan, H. Bin Wu, X.W. Lou, Metal–organic framework-assisted synthesis of compact Fe_2O_3 nanotubes in Co_3O_4 host with enhanced lithium storage properties, Nano-Micro Lett. 10 (2018) 1–9, https://doi.org/10.1007/s40820-018-0197-1.
[9] D. Wang, W. Zhou, R. Zhang, X. Huang, J. Zeng, Y. Mao, C. Ding, J. Zhang, J. Liu, G. Wen, MOF-derived Zn-Mn mixed oxides@carbon hollow disks with robust hierarchical structure for high-performance lithium-ion batteries, J. Mater. Chem. A 6 (2018) 2974–2983, https://doi.org/10.1039/c7ta10154f.
[10] M. Zheng, H. Tang, L. Li, Q. Hu, L. Zhang, H. Xue, H. Pang, Hierarchically nanostructured transition metal oxides for lithium-ion batteries, Adv. Sci. 5 (2018) 1700592, , https://doi.org/10.1002/advs.201700592.
[11] J. Cabana, L. Monconduit, D. Larcher, M.R. Palacín, Beyond intercalation-based Li-ion batteries: the state of the art and challenges of electrode materials reacting through conversion reactions, Adv. Mater. 22 (2010) 170–192, https://doi.org/10.1002/adma.201000717.
[12] M.V. Reddy, G.V. Subba Rao, B.V.R. Chowdari, Metal oxides and oxysalts as anode materials for Li ion batteries, Chem. Rev. 113 (2013) 5364–5457, https://doi.org/10.1021/cr3001884.
[13] C. Suchomski, B. Breitung, R. Witte, M. Knapp, S. Bauer, T. Baumbach, C. Reitz, T. Brezesinski, Microwave synthesis of high-quality and uniform 4 nm $ZnFe_2O_4$ nanocrystals for application in energy storage and nanomagnetics, Beilstein J. Nanotechnol. 7 (2016) 1350–1360, https://doi.org/10.3762/bjnano.7.126.
[14] A. Sarkar, L. Velasco, D. Wang, Q. Wang, G. Talasila, L. de Biasi, C. Kübel, T. Brezesinski, S.S. Bhattacharya, H. Hahn, B. Breitung, High entropy oxides for reversible energy storage, Nat. Commun. 9 (2018) 3400, , https://doi.org/10.1038/s41467-018-05774-5.
[15] N. Qiu, H. Chen, Z. Yang, S. Sun, Y. Wang, Y. Cui, A high entropy oxide ($Mg_{0.2}Co_{0.2}Ni_{0.2}Cu_{0.2}Zn_{0.2}O$) with superior lithium storage performance, J. Alloys Compd. 777 (2019) 767–774, https://doi.org/10.1016/j.jallcom.2018.11.049.
[16] J.-W. Yeh, S.-K. Chen, S.-J. Lin, J.-Y. Gan, T.-S. Chin, T.-T. Shun, C.-H. Tsau, S.-Y. Chang, Nanostructured high-entropy alloys with multiple principal elements: novel alloy design concepts and outcomes, Adv. Eng. Mater. 6 (2004) 299–303, https://doi.org/10.1002/adem.200300567.
[17] R. Djenadic, A. Sarkar, O. Clemens, C. Loho, M. Botros, V.S.K. Chakravadhanula, C. Kübel, S.S. Bhattacharya, A.S. Gandhi, H. Hahn, Multicomponent equiatomic rare earth oxides, Math. Res. Lett. 5 (2017) 102–109, https://doi.org/10.1080/21663831.2016.1220433.
[18] C.M. Rost, E. Sachet, T. Borman, A. Moballegh, E.C. Dickey, D. Hou, J.L. Jones, S. Curtarolo, J.P. Maria, Entropy-stabilized oxides, Nat. Commun. 6 (2015) 1–8, https://doi.org/10.1038/ncomms9485.
[19] D. Bérardan, S. Franger, A.K. Meena, N. Dragoe, Room temperature lithium superionic conductivity in high entropy oxides, J. Mater. Chem. A 4 (2016) 9536–9541, https://doi.org/10.1039/c6ta03249d.
[20] A. Sarkar, R. Djenadic, N.J. Usharani, K.P. Sanghvi, V.S.K. Chakravadhanula, A.S. Gandhi, H. Hahn, S.S. Bhattacharya, Nanocrystalline multicomponent entropy stabilised transition metal oxides, J. Eur. Ceram. Soc. 37 (2017) 747–754, https://doi.org/10.1016/j.jeurceramsoc.2016.09.018.
[21] A. Sarkar, R. Djenadic, D. Wang, C. Hein, R. Kautenburger, O. Clemens, H. Hahn, Rare earth and transition metal based entropy stabilised perovskite type oxides, J. Eur. Ceram. Soc. 38 (2018) 2318–2327, https://doi.org/10.1016/J.JEURCERAMSOC.2017.12.058.
[22] J. Dąbrowa, M. Stygar, A. Mikuła, A. Knapik, K. Mroczka, W. Tejchman, M. Danielewski, M. Martin, Synthesis and microstructure of the $(Co,Cr,Fe,Mn,Ni)_3O_4$ high entropy oxide characterized by spinel structure, Mater. Lett. 216 (2018) 32–36, https://doi.org/10.1016/j.matlet.2017.12.148.
[23] C. Wei, Y. Zhang, S.-J. Lee, L. Mu, J. Liu, C. Wang, Y. Yang, M. Doeff, P. Pianetta, D. Nordlund, X.-W. Du, Y. Tian, K. Zhao, J.-S. Lee, F. Lin, Y. Liu, Thermally driven mesoscale chemomechanical interplay in $Li_{0.5}Ni_{0.6}Mn_{0.2}Co_{0.2}O_2$ cathode materials, J. Mater. Chem. A 6 (2018) 23055–23061, https://doi.org/10.1039/C8TA08973F.
[24] F. Schipper, E.M. Erickson, C. Erk, J.-Y. Shin, F.F. Chesneau, D. Aurbach, Review—recent advances and remaining challenges for Lithium ion battery cathodes, J. Electrochem. Soc. 164 (2017) A6220–A6228, https://doi.org/10.1149/2.0351701jes.
[25] T. Ohzuku, Y. Makimura, Layered lithium insertion material of $LiCo_{1/3}Ni_{1/3}Mn_{1/3}O$ 2 for lithium-ion batteries, Chem. Lett. 30 (2001) 642–643, https://doi.org/10.1246/cl.2001.642.
[26] B. Xu, D. Qian, Z. Wang, Y.S. Meng, Recent progress in cathode materials research for advanced lithium ion batteries, Mater. Sci. Eng. R. Rep. 73 (2012) 51–65, https://doi.org/10.1016/j.mser.2012.05.003.
[27] M.-S. Balogun, W. Qiu, Y. Luo, H. Meng, W. Mai, A. Onasanya, T.K. Olaniyi, Y. Tong, A review of the development of full cell lithium-ion batteries: the impact of nanostructured anode materials, Nano Res. 9 (2016) 2823–2851, https://doi.org/10.1007/s12274-016-1171-1.
[28] E. Kamali Heidari, A. Kamyabi-Gol, M. Heydarzadeh Sohi, A. Ataie, Electrode materials for Lithium ion batteries: a review, JUFGNSM 51 (2018) 1–12, https://doi.org/10.22059/JUFGNSM.2018.01.01.
[29] J. Hassoun, F. Croce, I. Hong, B. Scrosati, Lithium-iron battery: Fe_2O_3 anode versus $LiFePO_4$ cathode, Electrochem. Commun. 13 (2011) 228–231, https://doi.org/10.1016/j.elecom.2010.12.020.
[30] S. Hariharan, V. Ramar, S.P. Joshi, P. Balaya, Developing a light weight lithium ion battery-an effective material and electrode design for high performance conversion anodes, RSC Adv. 3 (2013) 6386–6394, https://doi.org/10.1039/c3ra23244a.
[31] P.S. Veluri, S. Mitra, High-rate capable full-cell Lithium-ion battery based on a conversion anode and an intercalation cathode, ChemElectroChem. 4 (2017) 686–691, https://doi.org/10.1002/celc.201600681.
[32] P. Xiong, L. Peng, D. Chen, Y. Zhao, X. Wang, G. Yu, Two-dimensional nanosheets based Li-ion full batteries with high rate capability and flexibility, Nano Energy 12 (2015) 816–823, https://doi.org/10.1016/j.nanoen.2015.01.044.
[33] B. Zou, Q. Hu, D. Qu, R. Yu, Y. Zhou, Z. Tang, C. Chen, A high energy density full lithium-ion cell based on specially matched coulombic efficiency, J. Mater. Chem. A 4 (2016) 4117–4124, https://doi.org/10.1039/c6ta00069j.
[34] Y. Wang, Y. Wang, D. Jia, Z. Peng, Y. Xia, G. Zheng, All-nanowire based li-ion full cells using homologous Mn_2O_3 and $LiMn_2O_4$, Nano Lett. 14 (2014) 1080–1084, https://doi.org/10.1021/nl4047834.
[35] D. Alonso-Domínguez, M.L. López, L. García-Quintana, I. Álvarez-Serrano, C. Pico, M.L. Veiga, Lithium-ion full cell battery with spinel-type nanostructured electrodes, Nano-Structures Nano-Objects 11 (2017) 88–93, https://doi.org/10.1016/j.nanoso.2017.07.005.
[36] K. Kierzek, J. MacHnikowski, Factors influencing cycle-life of full Li-ion cell built from Si/C composite as anode and conventional cathodic material, Electrochim. Acta 192 (2016) 475–481, https://doi.org/10.1016/j.electacta.2016.02.019.
[37] S. Chae, M. Ko, K. Kim, K. Ahn, J. Cho, Confronting issues of the practical implementation of Si anode in high-energy lithium-ion batteries, Joule 1 (2017) 47–60, https://doi.org/10.1016/j.joule.2017.07.006.
[38] A.O. Kondrakov, H. Geßwein, K. Galdina, L. de Biasi, V. Meded, E.O. Filatova, G. Schumacher, W. Wenzel, P. Hartmann, T. Brezesinski, J. Janek, Charge-transfer-induced lattice collapse in Ni-rich NCM cathode materials during delithiation, J. Phys. Chem. C 121 (2017) 24381–24388, https://doi.org/10.1021/acs.jpcc.7b06598.
[39] L. de Biasi, A.O. Kondrakov, H. Geßwein, T. Brezesinski, P. Hartmann, J. Janek, Between Scylla and Charybdis: balancing among structural stability and energy density of layered NCM cathode materials for advanced lithium-ion batteries, J. Phys. Chem. C 121 (2017) 26163–26171, https://doi.org/10.1021/acs.jpcc.7b06363.
[40] F. Leng, C.M. Tan, M. Pecht, Effect of temperature on the aging rate of Li ion battery operating above room temperature, Sci. Rep. 5 (2015) 1–12, https://doi.org/10.1038/srep12967.
[41] Y. Sun, H.-W. Lee, Z.W. Seh, N. Liu, J. Sun, Y. Li, Y. Cui, High-capacity battery cathode prelithiation to offset initial lithium loss, Nat. Energy 1 (2016) 15008, , https://doi.org/10.1038/nenergy.2015.8.